

OPEN ACCESS

EDITED BY

Amir Abbas,
University of Gujrat, Pakistan

REVIEWED BY

Padmavathi Thiyagarajan,
Saveetha Engineering College, India
Adnan Asghar,
Universiti Utara Malaysia, Malaysia

*CORRESPONDENCE

Umair Khan,
✉ umair.khan@lau.edu.lb

RECEIVED 25 February 2024

ACCEPTED 18 April 2024

PUBLISHED 10 June 2024

CITATION

Chakraborty A, Saadeh R, Qazza A, Zomot N, Janapatla P, Khan U, Graywi M and Muhammad T (2024), On the thermal performance of radiative stagnation-point hybrid nanofluid flow across a wedge with heat source/sink effects and sensitivity analysis.

Front. Mater. 11:1391377.

doi: 10.3389/fmats.2024.1391377

COPYRIGHT

© 2024 Chakraborty, Saadeh, Qazza, Zomot, Janapatla, Khan, Graywi and Muhammad. This is an open-access article distributed under the terms of the [Creative Commons Attribution License \(CC BY\)](https://creativecommons.org/licenses/by/4.0/). The use, distribution or reproduction in other forums is permitted, provided the original author(s) and the copyright owner(s) are credited and that the original publication in this journal is cited, in accordance with accepted academic practice. No use, distribution or reproduction is permitted which does not comply with these terms.

On the thermal performance of radiative stagnation-point hybrid nanofluid flow across a wedge with heat source/sink effects and sensitivity analysis

Anomitra Chakraborty¹, Rania Saadeh², Ahmad Qazza², Naser Zomot², Pranitha Janapatla¹, Umair Khan^{3,4*}, Mohammad Graywi⁵ and Taseer Muhammad⁶

¹Department of Mathematics, National Institute of Technology Warangal, Warangal, India, ²Faculty of Science, Zarqa University, Zarqa, Jordan, ³Department of Mathematics, Faculty of Science, Sakarya University, Sakarya, Türkiye, ⁴Department of Computer Science and Mathematics, Lebanese American University, Byblos, Lebanon, ⁵Department of Civil Engineering, Faculty of Engineering and Built Environment, Universiti Kebangsaan Malaysia, Bangi, Selangor, Malaysia, ⁶Department of Mathematics, College of Science, King Khalid University, Abha, Saudi Arabia

The present article aims to examine the thermal performance and the sensitivity analysis of a $GO-TiO_2$ /water hybrid nanofluid in the presence of different nanoparticle shapes along with heat absorption and thermal radiation effects over a wedge geometry. Analyzing the effects of heat generation and radiation effects is one of the key studies conducted by researchers in various nanofluid flows over some required geometries. However, a combined study of these effects has yet to be studied over a moving wedge, and that combination defines the novelty of the work. Similarity transformations are implemented to the governing equations to obtain the final set of nondimensional equations, which are solved using the `bvp4c` code in MATLAB. The results obtained were in close agreement with the published results. The Nusselt number decreased with an increase in the heat source parameter (Q), and it increased with an increasing Hartree pressure gradient (β) and thermal radiation parameter (Rd). The sensitivity is statistically analyzed for the variations in radiation effect, heat source, and pressure gradient parameters on the Nusselt number. The high values for $R^2 = 99.99\%$ and $AdjR^2 = 99.96\%$ validate the ANOVA results obtained using a Box–Behnken design (BBD) model in the response surface methodology (RSM) with 14 degrees of freedom. The input parameters Rd and β show positive sensitivity, while Q shows negative sensitivity toward the skin friction. The Nusselt number proves to be most sensitive toward the pressure gradient parameter. TiO_2 , graphene (Gr), and the derivative forms of graphene, are gaining much importance due to their wide applications in the oil and petroleum industries. Thus, this study contributes to lubrication purposes, emulsion stabilizers, oxalic acid removal, anti-corrosive properties, etc.

KEYWORDS

nanofluid, wedge, radiation, sensitivity analysis, graphene

1 Introduction

Nanotechnology is the field of science that deals with nanometer-sized particles with a size range of 1–100 nm. Nanofluids have a higher thermal conductivity than ordinary fluids due to the addition of nanoparticles. They are mostly used in the smart computing and medical fields. In 1995, Choi and Eastman (1995) first revealed the presence of nanofluids to the scientific world. The Tiwari–Das and Buongiorno models (Buongiorno, 2005; Tiwari and Das, 2007) are the two types of nanofluid models used widely in current academic research. Hatami and Safari (2016) and Makinde and Aziz (2011) completed extensive studies on the nature of nanofluid flows over various geometries. Kumari et al. (2001), Chakraborty and Janapatla (2023) and Gorla et al. (2010) used vertical wedge geometry to study the steady and mixed convective flows of nanofluids.

With a structure mimicking a honeycomb, graphene (Gr) comprises single-layered sp^2 hybridized carbon atoms. After the oxidation process with the oxygen (O_2) atom, a multidimensional compound, graphene oxide (GO), is formed (Natalini and Sciubba, 1999). This compound was first prepared by oxidizing graphite in the presence of HNO_3 and KCl , by Baronet Benjamin Colline Brodie in 1859. At present, the modified Hummers method is implemented for the synthesis of GO (Kock and Herwig, 2004). The electrical conductivity of graphene was measured to be approximately $7200 S/m$ and at room temperature, and the thermal conductivity varies between 1800 – $5800 W/mK$ (Kuilla et al. (2010). Graphene is considered to be one of the strongest materials, with an intrinsic strength of $130 GPa$ and a breaking strength of $42 N/m$ (Lee et al., 2008). Graphene oxide is one of the most important additives for cement. Small amounts (0.03%) of GO can cause a 39%–57% increase in the flexural strength, increased compressive strength, and increased ductility, and the corrosion caused by microbes might be avoided by using GO (Mangadlao et al., 2015). Graphene oxide is a good emulsion stabilizer because it behaves as a colloidal surfactant due to its amphoteric nature (Kim et al., 2010).

The study of the radiation effect is one of the most important effects studies in academia for its wide range of applications in science and technology concerning heat and mass transfer of flows. Being implemented in nuclear waste extraction and separation processes, the study of convective heat transfer within fluid flow has gained importance among researchers. Some extensive and comprehensive studies were performed on the convective nature of the flows (Sivakumar et al., 2017). One study examined a magnetohydrodynamics (MHD) flow of ferro-liquid in the presence of two types of external effects, viz, viscous dissipative radiation effects with slip and convective boundary conditions along with the thermal radiation effect (Cheng, 1979). TiO_2 is a non-toxic, economical, stable ceramic material with a relatively high thermal conductivity (4.0 – $11.8 W m^{-1} K^{-1}$). The thermal behavior was studied in the presence of a heat source/sink for a copper-titanium oxide ($Cu-TiO_2$) hybrid nanofluid (Leong et al., 2018), and the results were concurrently compared to a conventional (Cu and TiO_2) nanofluid. The mathematical model of a nanofluid with based fluid (engine oil) and titanium dioxide nanoparticles (Vasheghani et al., 2013).

TABLE 1 Thermophysical properties of nanoparticles and base fluids.

Nanoparticles and base fluid	Density (ρ)	Specific heat (C_p)	Thermal conductivity (k)	Prandtl number (Pr)
TiO_2	4,250	686.2	8.9538	--
GO	1,800	717	5,000	--
Water	997.1	4,179	0.613	6.2

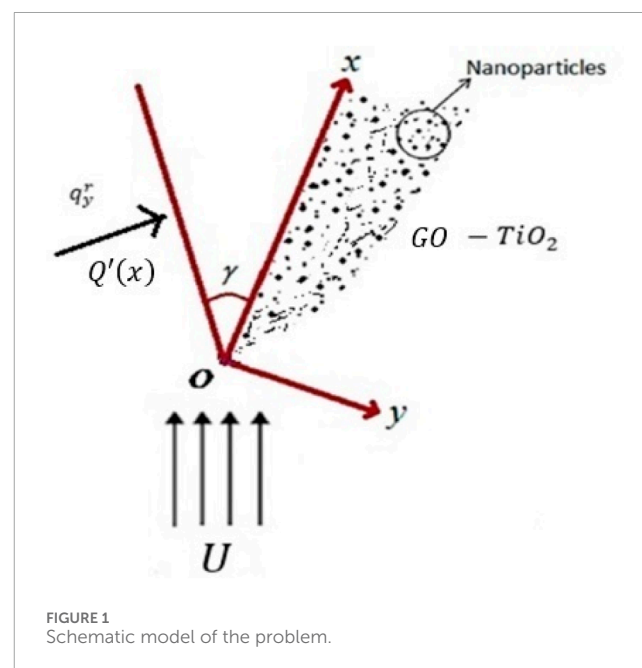


FIGURE 1 Schematic model of the problem.

The tool used by the present researchers to examine the extent of the effect of any parameter is the sensitivity analysis, which gained its importance for the wide range of applications in control theory and nuclear industries. Empirical relationships are formed to correlate the input and the output responses with the help of ANOVA using the response surface methodology (RSM). The primary focus of the study was to implement a sensitivity analysis for the Newtonian nanofluid study. In this context, using triangle-shaped obstacles, Rashidi et al. (2015) conducted a sensitivity analysis using the RSM. It was observed that the wedge angle parameter proved to be more sensitive to the Nusselt number than the skin friction coefficient. Darbari et al. (2016) studied the flow through a channel and evaluated the sensitivity analysis of the nanofluid flow properties. Reynold's number was found to be most sensitive to the entropy generation. The RSM was utilized to investigate the Casson fluid flow, and, as expected, Abdelmalek et al. (2020) found that positive sensitivity prevails for a Nusselt number with increasing magnetic parameters.

The combined effects of magnetic effects, the Falkner–Skán parameter (m), and thermal radiation for the hybrid nanofluid of graphene oxide and titanium in water over a wedge has been studied in this article and has not yet been addressed

TABLE 2 Thermophysical properties of hybrid nanofluids (Maïga et al., 2004).

Properties	Expression
Dynamic viscosity	$\mu_{hnf} = \begin{cases} \frac{\mu_f}{(1-\phi_1-\phi_2)^{2.5}}, & \text{if both are spherical} \\ (1 + A_1(\phi_1 + \phi_2) + B_1(\phi_1 + \phi_2)^2)\mu_f, & \text{if both are non-spherical} \end{cases}$
Density	$\rho_{hnf} = (1 - \phi_2)[(1 - \phi_1)\rho_f + \phi_1\rho_1] + \phi_2\rho_2$
Heat capacity	$(\rho C_p)_{hnf} = (1 - \phi_2)[(1 - \phi_1)(\rho C_p)_f + \phi_1(\rho C_p)_1] + \phi_2(\rho C_p)_2$
Thermal conductivity	$\frac{k_{hnf}}{k_f} = \frac{k_2 + (n_2 - 1)k_{nf} - (n_2 - 1)\phi_2(k_{nf} - k_2)}{k_2 + (n_2 - 1)k_{nf} + \phi_2(k_{nf} - k_2)}$ And $\frac{k_{nf}}{k_f} = \frac{k_1 + (n_1 - 1)k_f - (n_1 - 1)\phi_1(k_f - k_1)}{k_1 + (n_1 - 1)k_f + \phi_1(k_f - k_1)}$ <i>hnf</i> : Hybrid nanofluid; <i>nf</i> : nanofluid; <i>f</i> : Base fluid

TABLE 3 Empirical shape factor values [(Dinarvand et al., 2019), (Hassan et al., 2022)].

Shapes	Shape factors (n_1, n_2)	Sphericity (ξ)	A_1	B_1
Spherical	3	1	2.5	6.5
Brick	3.7	0.81	1.9	471.4
Platelet	5.7	0.52	37.1	612.6

TABLE 4 Comparison of $f''(0)$ values for various Falkner–Skán parameter values.

m	Yih (1998)	White and Majdalani (2006)	Ishak et al. (2007)	Yacob et al. (2011)	Nadeem et al. (2018)	Present study
0.0	0.4696	--	0.4696	0.4696	0.4696	0.4696
0.2	0.802125	--	0.8021	0.8021	0.802125	0.8021
0.4	--	--	--	--	0.976824	0.976825
0.5	--	--	--	1.0389	1.0389	1.0389
1.0	1.232588	1.23259	1.2326	1.2326	1.232587	1.23259

in the literature, indicating the novelty of our work. MATLAB bvp4c has been used to solve the set of ordinary differential equations obtained by similarity transformations. The results were compared with the previously published results and found to be in good agreement. The applications of graphene and its derivatives as emulsion stabilizers, anti-corrosion coatings, etc., in the oil and petroleum industries are the motivation for conducting the present study.

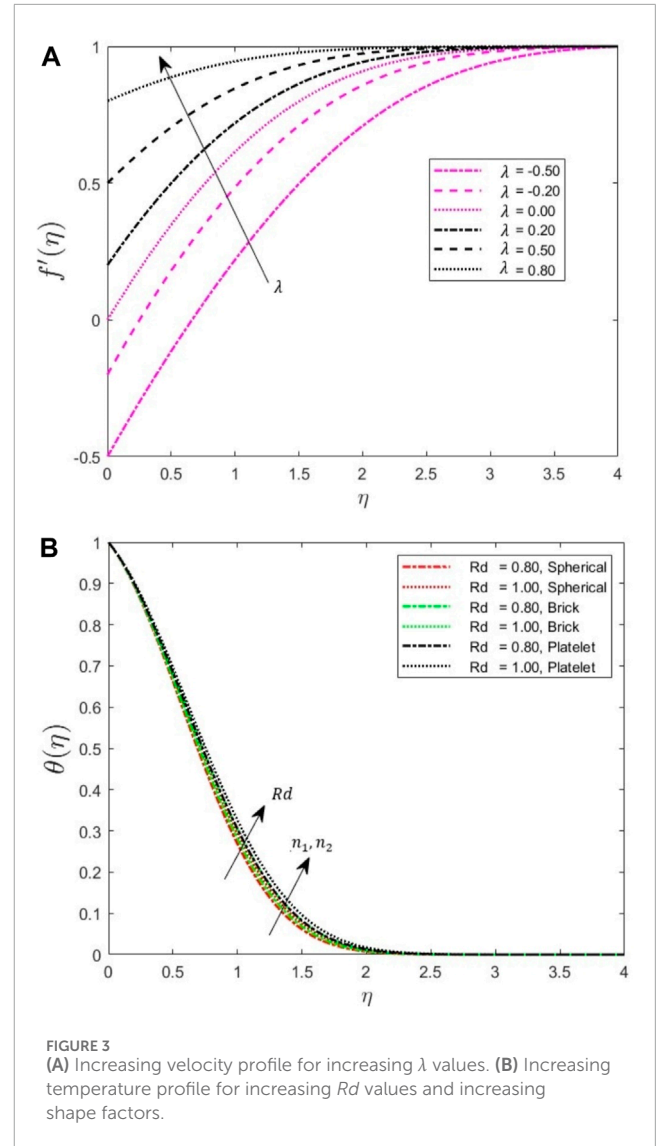
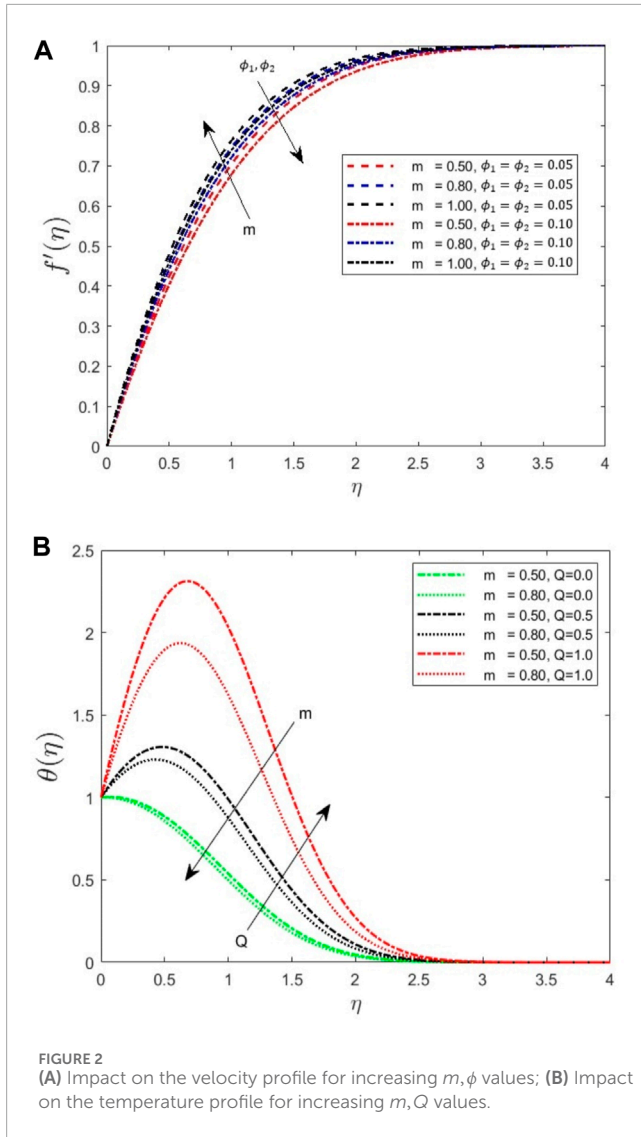
2 Problem formulation

A steady, laminar, and 2D incompressible flow is considered in the present study with an aqueous solution of the $GO - TiO_2$ /water hybrid nanofluid over a static or moving wedge. Graphene oxide is the first nanoparticle denoted by the subscript 1, and titanium oxide is the second nanoparticle denoted by 2 in the

subscript. The thermophysical properties of the nanoparticles are presented in Table 1 as considered in the temperature range of 25°C–30°C (Dinarvand et al., 2019; Sundar et al., 2020; Verma et al., 2022).

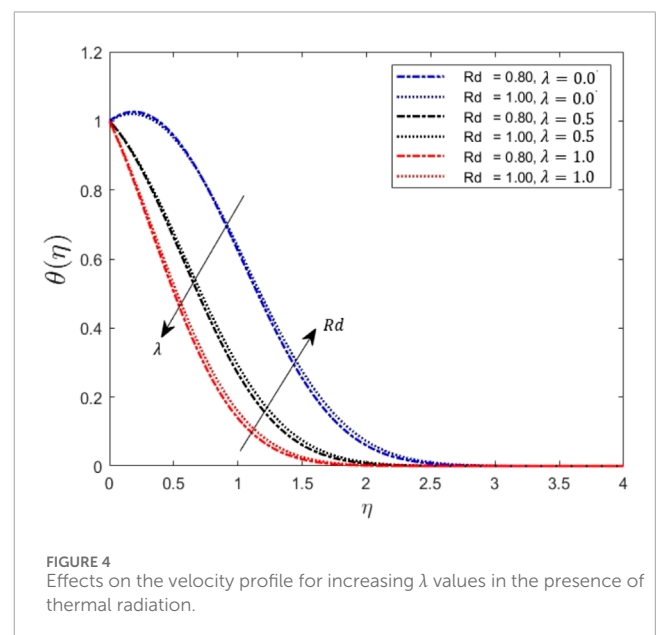
Figure 1 shows the schematic representation of the problem considered for our study. The x -axis is taken along the wedge surface, and the free stream velocity is considered $U(x) = ax^m$, while for the moving wedge, the velocity is considered $u_w = U_w x^m$. Along with the boundary layer approximations, the Tiwari–Das model for nanofluids and Bernoulli’s equations have been implemented in the governing set of partial differential equations (PDEs) for our problem. The thermophysical properties of the hybrid nanofluids can be calculated from the properties of the individual nanoparticles and base fluids from the information provided in Table 2 (Maïga et al., 2004).

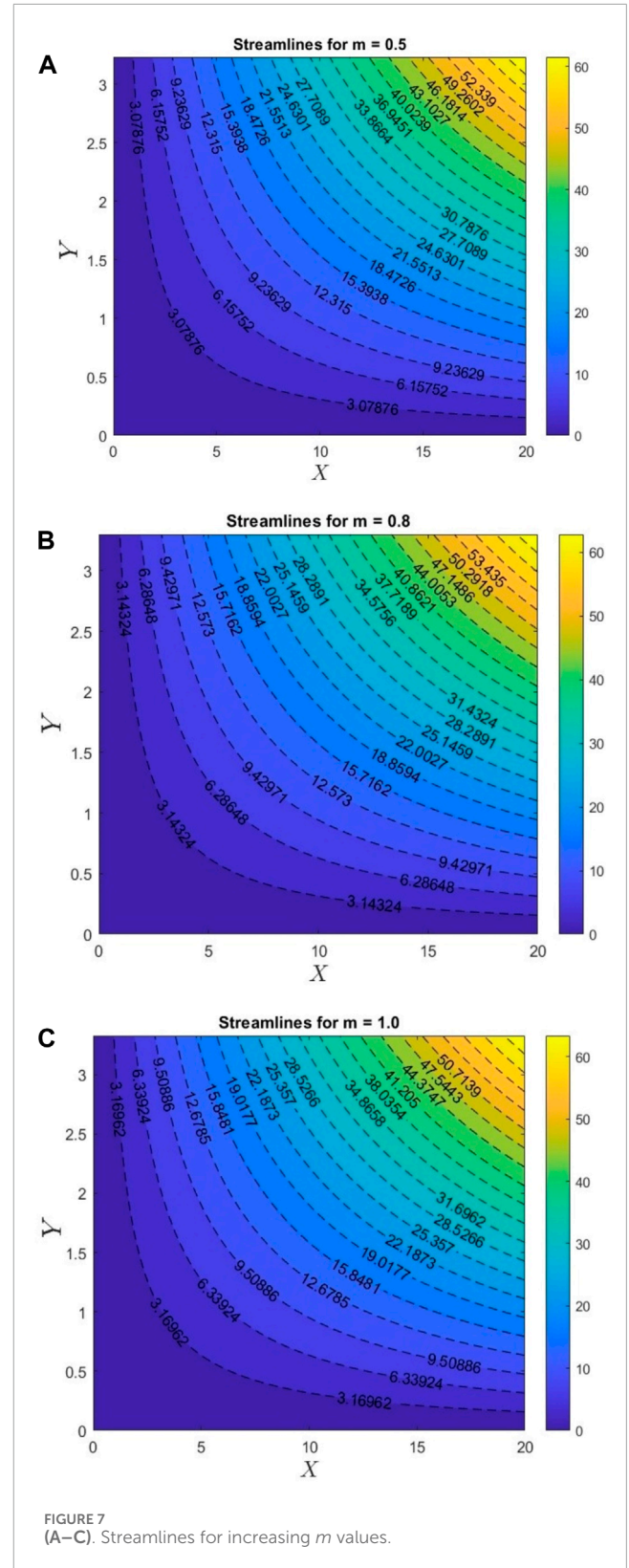
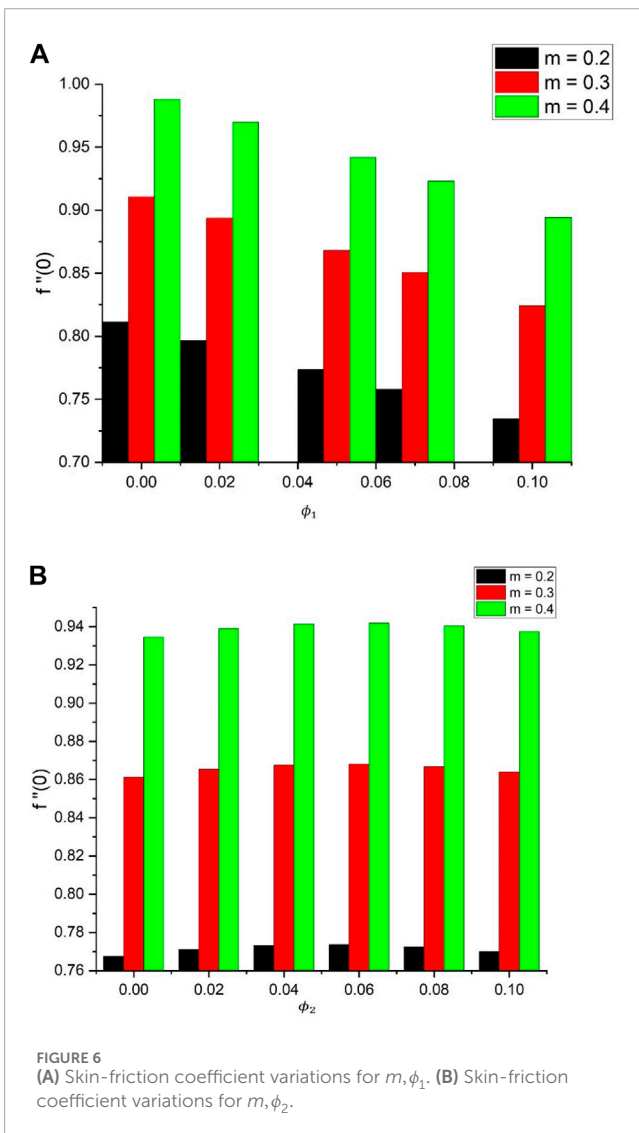
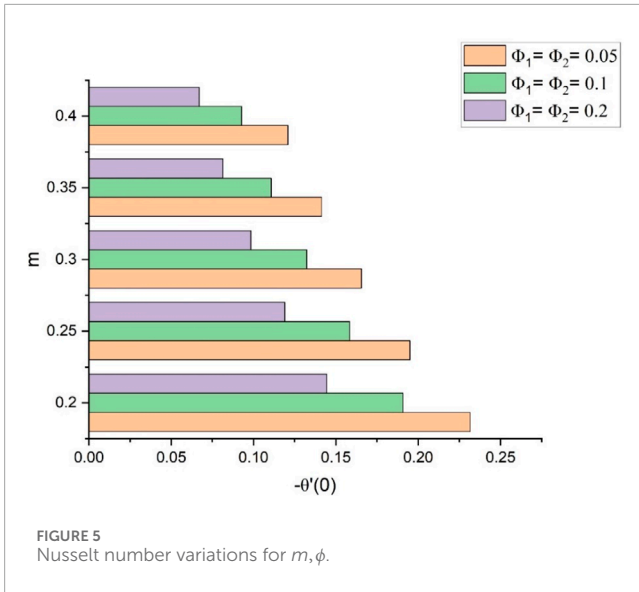
The assumptions considered for our problem are as follows:



- We see a variable surface temperature of the wedge as $T_w(x) = T_\infty + T_0x^{2m-1}$, and the ambient temperature of the hybrid nanofluid is given by T_∞ .
- The free stream velocity is given by $U(x) = ax^m, (a > 0)$, while $Q'(x) = Q_0x^{m-1}, Q_0 > 0$ is the constant heat production in the system.
- We have $m = \frac{\beta_1}{2-\beta_1}$ as the wedge angle parameter, and $\beta_1 = \frac{\Omega}{\pi}$, where Ω is the wedge angle. Here, the range for m is $[0, 1]$, where $m = 0$ indicates a horizontal plate, whereas $m = 1$ represents a vertical wedge.
- Complete thermal equilibrium is maintained between the nanoparticles and the base fluids, and no slips occur between them.
- In preparing the hybrid nanofluid, graphene oxide was first added to the base fluid (water), and later, titanium was added to the mixture, now a mono nanofluid, as the second nanoparticle.

In Table 2, we have computed the thermal conductivity of the nanofluids k_{nf} and k_{hnf} using the available value





of thermal conductivity of the base fluid k_f using the Hamilton–Crosser model (Ghadikolaie et al., 2017). Table 3 denotes the empirical shape factor values for the nanoparticles.

The equations governing the flow are as follows:

TABLE 5 ANOVA for Nusselt number.

Source	DF	Adjusted SS	Adjusted MS	F-value	p-value
Model	9	7.25863	0.80651	4245.27	0.000
Linear	3	7.22173	2.40724	12671.07	0.000
Rd	1	0.24129	0.24129	1270.09	0.000
Q	1	1.81085	1.81085	9531.83	0.000
β	1	5.16959	5.16959	27211.30	0.000
Square	3	0.02580	0.00860	45.27	0.000
Rd × Rd	1	0.00001	0.00001	0.04	0.850
Q × Q	1	0.00212	0.00212	11.18	0.020
β × β	1	0.02236	0.02236	117.72	0.000
Interaction	3	0.01110	0.00370	19.47	0.003
Rd × Q	1	0.00088	0.00088	4.62	0.084
Rd × β	1	0.00950	0.00950	50.03	0.001
Q × β	1	0.00071	0.00071	3.76	0.110
Error	5	0.00095	0.00019	--	--
Lack-of-fit	3	0.00095	0.00032	*	*
Pure error	2	0.00000	0.000000	--	--
Total	14	7.25958	--	--	--
S = 0.0137833 R ² = 99.99%		R ² = 99.99%		Adj R ² = 99.96%	

$$\frac{\partial u}{\partial x} + \frac{\partial v}{\partial y} = 0. \tag{1}$$

$$u \frac{\partial u}{\partial x} + v \frac{\partial u}{\partial y} = U(x) \frac{dU(x)}{dx} + \frac{\mu_{hnf}}{\rho_{hnf}} \frac{\partial^2 u}{\partial y^2}. \tag{2}$$

$$u \frac{\partial T}{\partial x} + v \frac{\partial T}{\partial y} = \frac{k_{hnf}}{(\rho C_p)_{hnf}} \frac{\partial^2 T}{\partial y^2} - \frac{\partial}{\partial y} \left(\frac{1}{(\rho C_p)_{hnf}} q_y^r \right) + \frac{Q'(x)}{(\rho C_p)_{hnf}} (T - T_\infty). \tag{3}$$

The boundary conditions are as follows (Dinarvand et al., 2019; Maïga et al., 2004):

$$v = 0; u = u_w(x); T = T_w \text{ at } y = 0. \tag{4}$$

$$u \rightarrow U(x); T \rightarrow T_\infty \text{ as } y \rightarrow \infty. \tag{5}$$

Using Rosseland’s approximation, q_y^r is the radiative heat flux given by

$$q_y^r = -\frac{4\sigma^*}{3k^*} \frac{\partial T^4}{\partial y}. \tag{6}$$

Here, k^* is Rosseland’s mean absorption coefficient, and σ^* is the Stefan–Boltzmann constant. While assuming negligible

temperature differences, Eq. (10) reduces to

$$\frac{\partial q_y^r}{\partial y} = -\frac{16\sigma^* T_\infty^3}{3k^*} \frac{\partial^2 T}{\partial y^2}. \tag{7}$$

The set of nondimensional similarity transformations is given by Kock and Herwig (2004) and Madhu et al. (2024):

$$\psi = \sqrt{\frac{2xv_f U(x)}{m+1}} f(\eta); \quad \eta = y \sqrt{\frac{(m+1)U(x)}{2xv_f}}; \quad \theta(\eta) = \frac{T - T_\infty}{T_w(x) - T_\infty}; \tag{8}$$

The stream function $\psi(x, y)$ can be defined as

$$u = \frac{\partial \psi}{\partial y}; \quad v = -\frac{\partial \psi}{\partial x}. \tag{9}$$

On incorporating Eqs 11, 13 into Eqs 5–9, we obtain

$$A_1 f''' + \frac{2m}{m+1} (1 - f'^2) + ff'' = 0. \tag{10}$$

$$\theta'' \left(\frac{k_{hnf}}{k_f} + Rd \right) + Pr \left(\frac{1}{A_2} (f\theta' - (3\beta_1 - 2)f'\theta) + \frac{2}{(m+1)} QA_2 \theta \right) = 0. \tag{11}$$

TABLE 6 Experimental design for coded and real values.

Exp. No.	Coded values			Real values			$Re_x^{-1/2}Nu_x$
	A	B	C	Rd	Q	β	
1	-1	0	1	0.6	0.3	1.4	3.159797
2	-1	0	-1	0.6	0.3	1.0	1.657961
3	0	-1	1	0.8	0.1	1.4	3.842938
4	-1	-1	0	0.6	0.1	1.2	2.763997
5	1	0	-1	1.0	0.3	1.0	1.913439
6	0	0	0	0.8	0.3	1.2	2.508967
7	0	0	0	0.8	0.3	1.2	2.508967
8	0	1	-1	0.8	0.5	1.0	1.255962
9	0	1	1	0.8	0.5	1.4	2.898815
10	-1	1	0	0.6	0.5	1.2	1.861398
11	0	-1	-1	0.8	0.1	1.0	2.253525
12	1	0	1	1.0	0.3	1.4	3.610253
13	0	0	0	0.8	0.3	1.2	2.508967
14	1	1	0	1.0	0.5	1.2	2.173477
15	1	-1	0	1.0	0.1	1.2	3.135346

along with the boundary conditions

$$f(\eta) = 0; \quad f'(\eta) = \lambda; \quad \theta(\eta) = 1 \quad \text{at} \quad \eta = 0. \quad (12)$$

$$f'(\eta) \rightarrow 1; \quad \theta(\eta) \rightarrow 0 \quad \text{as} \quad \eta \rightarrow \infty. \quad (13)$$

The quantities can be defined as

$$Pr = \frac{\nu}{\alpha}; \quad Rd = \frac{16\sigma^* T_\infty^3}{3k_f k^*}; \quad Q = \frac{Q_0}{(\rho C_p)_f a}; \quad \lambda = \frac{U_w}{a}. \quad (14)$$

Here, Pr is the Prandtl number, Rd is the radiation parameter, Q is the heat generation parameter, and λ is the velocity ratio parameter.

In addition, we have

$$A_1 = \frac{\mu_{hnf}}{\mu_f} \{ (1 - \phi_2) [(1 - \phi_1) + \phi_1 \rho_1 / \rho_f] + \phi_2 \rho_2 / \rho_f \}^{-1}.$$

$$A_2 = [(1 - \phi_2) [(1 - \phi_1) + \phi_1 (\rho C_p)_1 / (\rho C_p)_f] + \phi_2 (\rho C_p)_2 / (\rho C_p)_f]^{-1}.$$

The drag coefficient C_f and Nusselt number Nu_x are given by

$$C_f = \frac{\tau_w}{\rho_f U^2}; \quad Nu_x = \frac{x q_w}{k_f (T_w - T_\infty)}. \quad (15)$$

In this context, τ_w is the surface shear stress, and q_w is the surface heat flux. These quantities can be defined as

$$\tau_w = \mu_{hnf} \left[\frac{\partial u}{\partial y} \right]_{y=0}; \quad q_w = -k_{hnf} \left[\frac{\partial T}{\partial y} \right]_{y=0} + q''_{y(y=0)}. \quad (16)$$

Now, using the similarity transformation (8) into Eq. 16, we get the following reduced form as follows:

$$\left(\frac{2}{m+1} \right)^{1/2} C_f Re_x^{1/2} = \frac{\mu_{hnf}}{\mu_f} f''(0).$$

$$\left(\frac{2}{m+1} \right)^{1/2} Nu_x Re_x^{-1/2} = - \left(\frac{k_{hnf}}{k_f} + Rd \right) \theta'(0). \quad (17)$$

3 Numerical method

The governing set of Eqs 1–3 is converted to a set of coupled nonlinear ordinary differential equations (ODEs) Eqs 10, 11 using the similarity transformations and the theory concerning the boundary layer. The MATLAB `bvp4c` method implements the Lobatto IIIA method as the base method used to obtain C^1 solutions. The uniform accuracy of the solutions up to the fourth order in the chosen interval of integration is one of the key reasons for using the `bvp4c` method. The error of tolerance chosen for the present method is 10^{-10} . In Table 4, we have compared the $f''(0)$ values for water as the base fluid, in the absence of heat generation and radiation terms ($Q = Rd = 0$) and assuming $\phi_1 = \phi_2 = 0$, for a static wedge ($\lambda = 0$). The results had a very good correlation to the results of Yih (1998), White and Majdalani (2006), Ishak et al. (2007), Yacob et al. (2011), and Nadeem et al. (2018), which validates our code.

4 Results and discussion

The present study has been conducted in the presence of a magnetic field and thermal radiation for a GrO - TiO_2 /VPO hybrid nanofluid in the light of empirical shape factors that vary from spherical to lamina. The entire study has been conducted with values of the governing parameters: $\beta_1 = 1.0$; $Q = 0.5$; $Rd = 1.0$, $\phi_1 = \phi_2 = 0.05$ in the context of a static wedge ($\lambda = 0$) if not mentioned otherwise. The ranges of the parameters used are $1.0 \leq \beta_1 \leq 1.4$; $0.1 \leq Q \leq 0.5$; $0.6 \leq Rd \leq 1.0$, $0.01 \leq \phi_1, \phi_2 \leq 0.05$.

In Figure 2A, the effects of the Falkner–Skan parameter and the nanoparticle volume fraction values on the velocity profiles for a static wedge have been upheld. In the presence of spherical-shaped nanoparticles ($n_1 = n_2 = 3$), we can observe that the dimensionless velocity increases with an increasing parameter m , along with a reverse trend for the case of increasing ϕ_1, ϕ_2 values. The increase in the Falkner–Skan parameter causes the pressure gradient to increase, and it increases both the momentum boundary layer thickness and the velocity profile of the fluid. Increasing the nanoparticle volume fraction values causes an increase in the nanoparticle concentration in the fluid, reducing the overall velocity profile of the fluid.

Increasing the values of the Falkner–Skan parameter causes an increase in the thermal boundary layer thickness, which, in turn, causes the temperature of the fluid to decrease, and

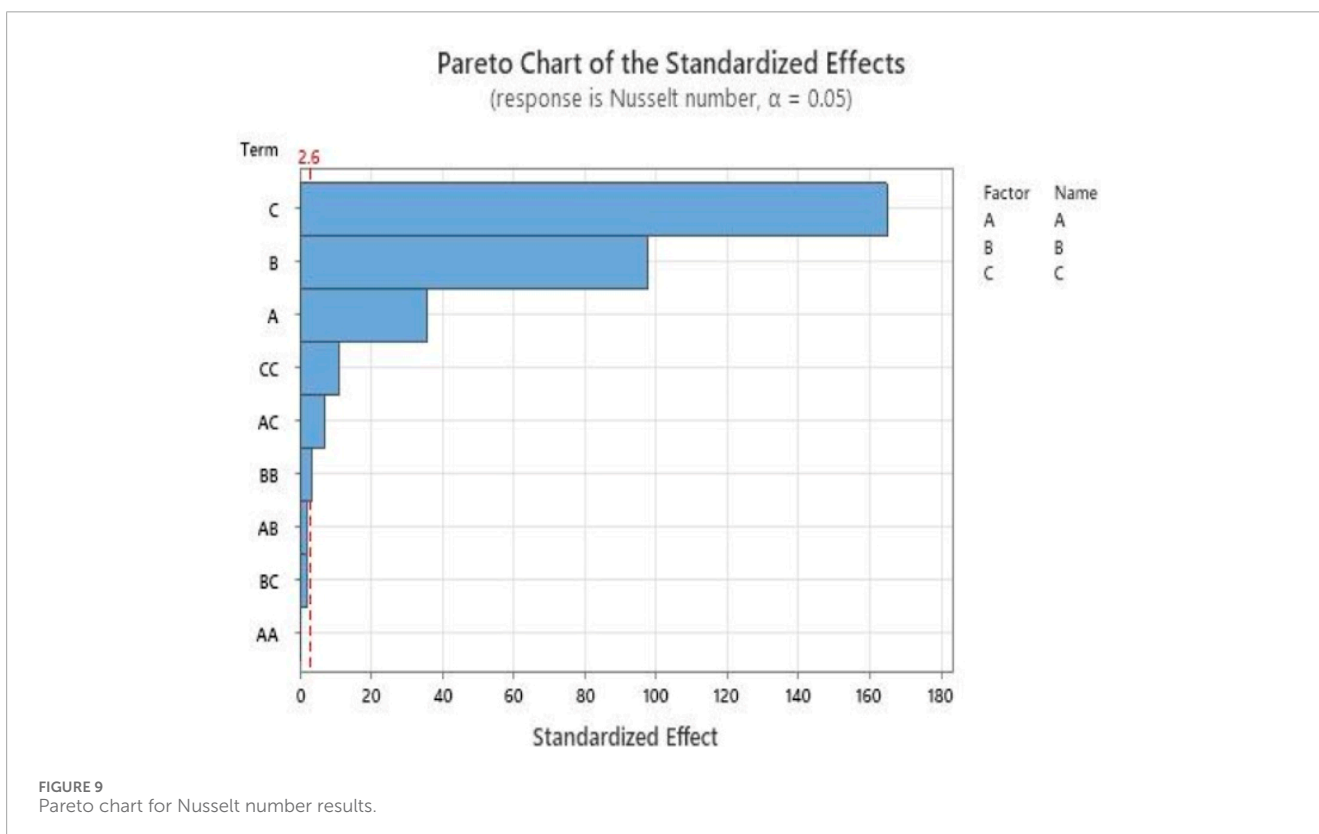
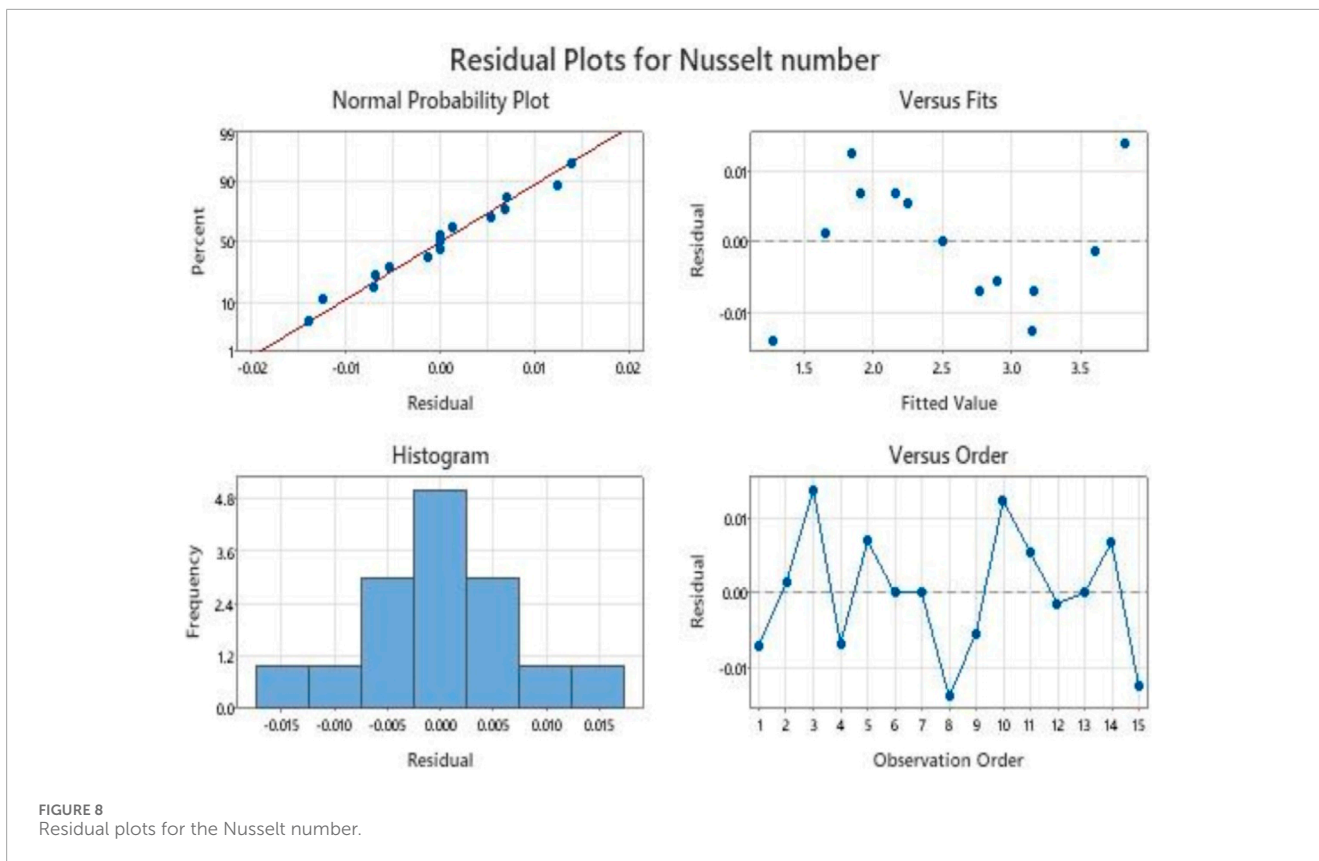


TABLE 7 Experimental designing for the factors and its levels.

Continuous factors	Coded symbols	Levels		
		Low (-1)	Medium (0)	High (1)
$0.6 \leq Rd \leq 1.0$	A	0.6	0.8	1.0
$0.1 \leq Q \leq 0.5$	B	0.1	0.3	0.5
$1.0 \leq \beta \leq 1.4$	C	1.0	1.2	1.4

this phenomenon has been upheld in Figure 2B. Increased heat generation parameter values cause more thermal energy to dissipate in the fluid, and this causes the thickness of the thermal boundary layer to decrease. This results in an increase in the temperature profile of the fluid; the validation of this fact is shown in Figure 2B.

In our study λ represents the velocity with which the wedge moves in the fluid. Hence, as the velocity of the wedge increases, due to the no-slip conditions, the layer of the fluid adjacent to the wedge surface also starts to accelerate, resulting in superposing the velocity along with the existing velocity of the fluid. Thus, for a nanofluid-saturated medium, as the velocity of the wedge increases, the velocity profile for the fluid flow system increases, as shown in Figure 3A.

The variation in the temperature profile for the increasing radiation parameter values and empirical shape factor of the nanoparticles has been represented in Figure 3B. Increasing the thermal radiation parameter Rd increases the convective flow, which in turn increases the velocity of the fluid. We observe that the thermal boundary layer thickness increases because the heat transfer increases. The temperature distribution is enhanced with an increase in the thermal radiation parameter. Owing to a higher surface area exposed in the fluid flow process, the thermal conductivity increases more for brick and platelet shapes than for spherical shapes. Hence, the temperature profiles are higher for higher shape values.

The increasing radiation parameter also increases the temperature profile of the fluid because, for a higher thermal conductivity, the fluid temperature increases, and, hence, the θ values are maximum for platelet and minimum for spherical shapes. Physically, the velocity of the wedge increases within the fluid flow system, and the thermal boundary layer thickness increases rapidly, causing the temperatures to fall subsequently. This is shown in Figure 4.

Figure 5 shows that the Nusselt number decreases as the Falkner–Skan parameter and nanoparticle volume fraction increase. As the pressure gradient increases, the flow velocity increases, and the density of the flow medium is reduced. This, in turn, increases the thermal diffusivity of the system. The heat transfer rate is found to be inversely proportional to the thermal diffusivity of the system, and thus, the Nusselt number decreases with increasing parameter m .

We see the increasing Nusselt number values when the heat generation parameter increases. Figure 6A, B represents the skin friction coefficient variations for an increasing Falkner–Skan parameter along with increasing nanoparticle volume fraction values for both nanoparticles with spherical shapes. The increasing pressure gradient parameter increases the wall shear

stress, while a reverse effect is observed for increasing volume fractions.

Figures 7A–C represent the streamlines for $m = 0.5, 0.8, 1.0$, that is, increasing the Falkner–Skan parameter during the fluid flow in a medium saturated with hybrid nanofluid. The increasing values of the streamlines denote that the flow is heavier away from the surface of the wedge than the flow near the wedge surface. In the stream plots for two different parameter values, we can observe that the corresponding streamline values are increasing, validating the fact that the velocity profile increases with an increasing pressure gradient parameter.

5 Response surface methodology (RSM)

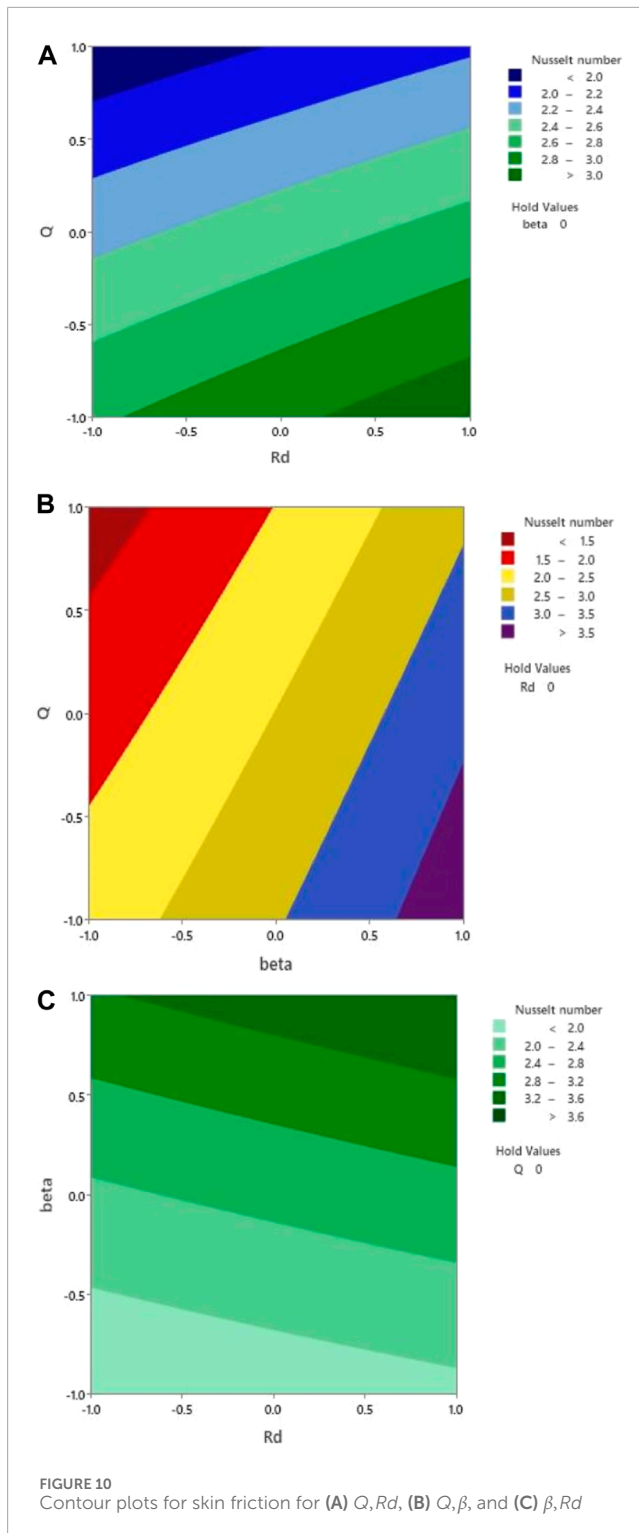
Analyzing any particular data set for its significance in influencing any response is a key role of any boundary layer mode experimental design. Such experimental models can be seen in the literature, such as response surface methodology and factorial designing using the central composite design (CCD) or the Box–Behnken design (BBD). In accordance with the numerical data evaluated, it can be observed that two of three quantities, namely, radiation parameter and pressure gradient, affect and increase the Nusselt number $Re_x^{-1/2}Nu_x$ but the heat source parameters reduce it. Among them, the most significant factor affecting the heat transfer rate can be determined by statistical data analysis. In this article, we have implemented the BBD model with three continuous factors, Rd, Q, β . The general form of correlation between the input parameters (Rd, Q, β) and the response parameter $Re_x^{-1/2}Nu_x$ can be written as:

$$Re_x^{-1/2}Nu_x = \alpha_0 + \alpha_1A + \alpha_2B + \alpha_3C + \alpha_{11}A^2 + \alpha_{22}B^2 + \alpha_{33}C^2 + \alpha_{12}AB + \alpha_{13}AC + \alpha_{23}BC. \quad (18)$$

Here, A, B, C are the coded symbols corresponding to the input parameters shown in Table 3. These α'_i, α'_{ij} are the regression coefficients to be determined by RSM using 20 experimental runs and 19 degrees of freedom. The coefficients will be determined using MINITAB software.

5.1 Analysis of variance (ANOVA)

The regression model values are determined by the ANOVA, along with the F-test, T-tests, and the p -values. These regression values are mentioned in Table 5. The F-test determines the variance



of the data, and the cases for F-values greater than 1 are considered to be significant for the input data to be correct. The level of significance for our data is 0.05, and outcomes with p -values less than 0.05 are considered statistically significant. Values greater than 0.05 are neglected in the output responses. Therefore, we will neglect the A^2, AB and BC terms in our model. The precision of the model is highlighted in Table 6 and Figure 8. The reduced expression (22)

using the ANOVA from Table 6 is as follows:

$$Re_x^{-1/2} Nu_x = 2.50987 + 0.17367A - 0.47577B + 0.80386C - 0.02398B^2 + 0.07783C^2 + 0.04874AC. \quad (19)$$

The model proves its goodness of fit by addressing the coefficient of determination determined by the $R^2 = 99.99\%$ and $AdjR^2 = 99.96\%$ values for the Nusselt number values as mentioned in Table 6.

The Pareto chart in Figure 9 represents the decreasing order of the standardized effects or the F-values for our data, and the red dotted line indicates significance. The terms to the right of the line are significant, and the terms to the left of the line are ignored for better results. Hence the A^2, AB and BC terms are omitted according to Figure 9, validating the P-test and F-test results in Table 7. The S-value in Table 5 indicates the variation of the results from the true response surface and has the units of the response variable. Hence, the small S-value determines the model chosen for our study and determines the response variable quite well. Also, these high values of R^2 and $AdjR^2$ indicate a very good fit of our model to the given data. The $PredR^2 = 96.79\%$ indicates a very high predictability rate of responses for new observations. In Figure 8, the residual plot versus fits shows data points evenly spread about the centerline, and the points are close to 0. Hence, the model chosen here meets the assumptions. The points in the residual versus order plot fall randomly on either side of the centerline with no particular pattern, signifying the independence of the data points. The normal probability plot indicates the residual to be normally distributed, and the probability plot shown in Figure 8 resembles a straight line; hence, the model is a good fit to all assumptions.

The contour plots in Figure 10 represent the behavioral patterns of the Nusselt number for increasing radiation effect, pressure gradient, and heat source effects. From Figure 10A, we can observe that the highest values of the Nusselt number indicated by dark green occur for the lowest heat source parameter values and the highest radiation parameter values. Hence, it indicates that the Nusselt number increases with increasing Rd values. In Figure 10B, we also see that the lowest values of the Nusselt number lie in the maroon region and the highest values lie in the purple region, which explains that $Re_x^{-1/2} Nu_x$ increases for increasing β values while it decreases with Q . These facts are also supported by Figure 10C.

The surface plots in Figure 11 also represent the fact described in Figure 10 in a more explanatory way, where the decreasing slopes of the surfaces in all three subfigures indicate that $Re_x^{-1/2} Nu_x$ decreases with the increasing Q , while it increases for Rd, β . Figure 12 represents the normalized effects of the input parameters on the response variable.

6 Sensitivity analysis

The goal of this study is to determine how the uncertainties corresponding to the system inputs can be correlated to the response to the physical problem. It provides an effective and concrete justification of how much the continuous factors influence the response parameter. The flow chart of the analysis is provided in Figure 13. In this analysis, we need to evaluate the partial derivatives of Eq. (19) with respect to the input-independent parameters (Rd, Q, β) and evaluate the derivatives

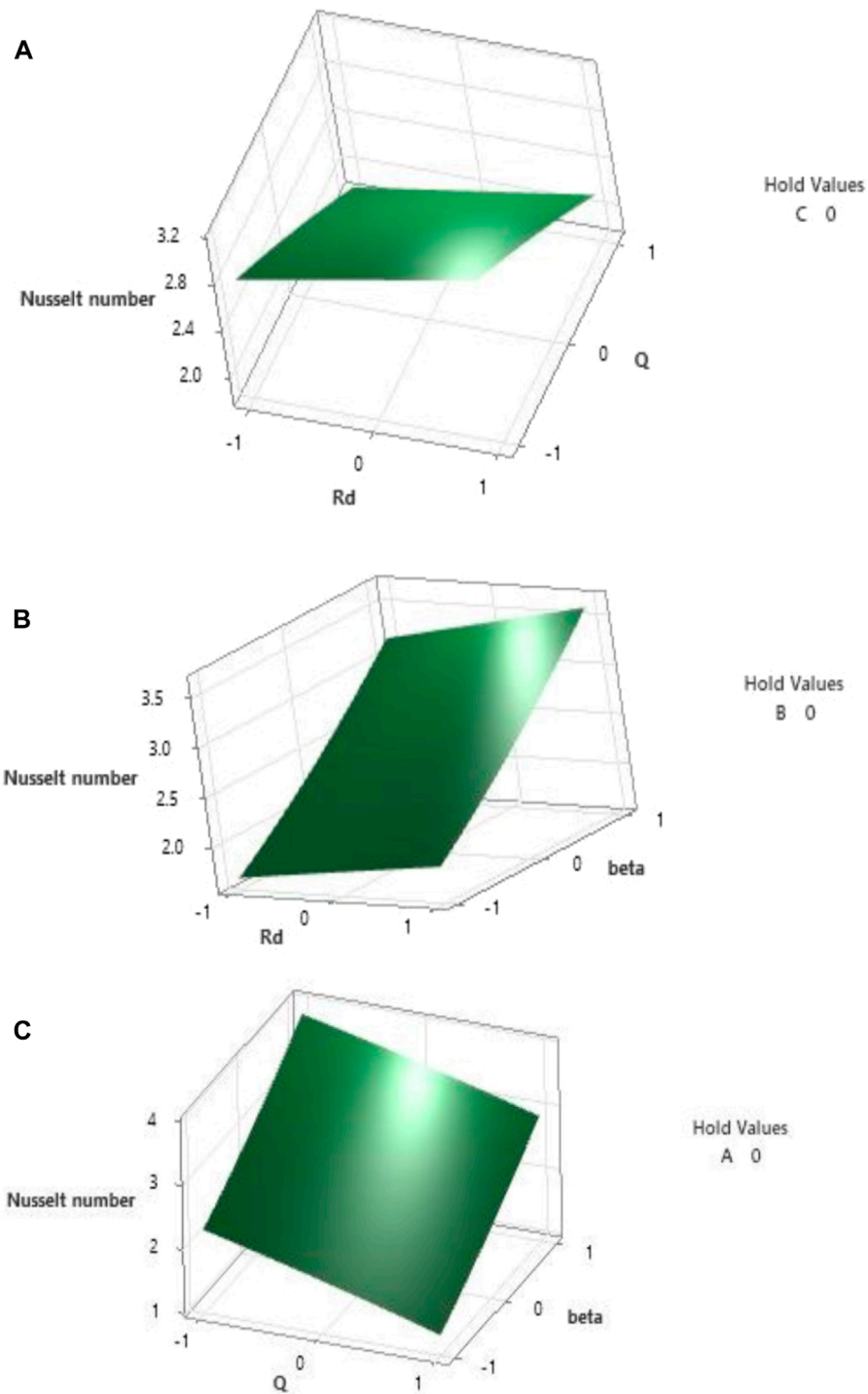


FIGURE 11 3D surface plots for the Nusselt number for (A) Rd, Q , (B) Rd, β , and (C) β, Q .

at the three different levels mentioned in Table 4. The reduced expressions are

$$\frac{\partial(Re_x^{-1/2}Nu_x)}{\partial A} = 0.17367 + 0.04874C. \quad (20)$$

$$\frac{\partial(Re_x^{-1/2}Nu_x)}{\partial B} = -0.47577 - 0.04796B. \quad (21)$$

$$\frac{\partial(Re_x^{-1/2}Nu_x)}{\partial C} = 0.80386 + 0.04874A + 0.15566C. \quad (22)$$

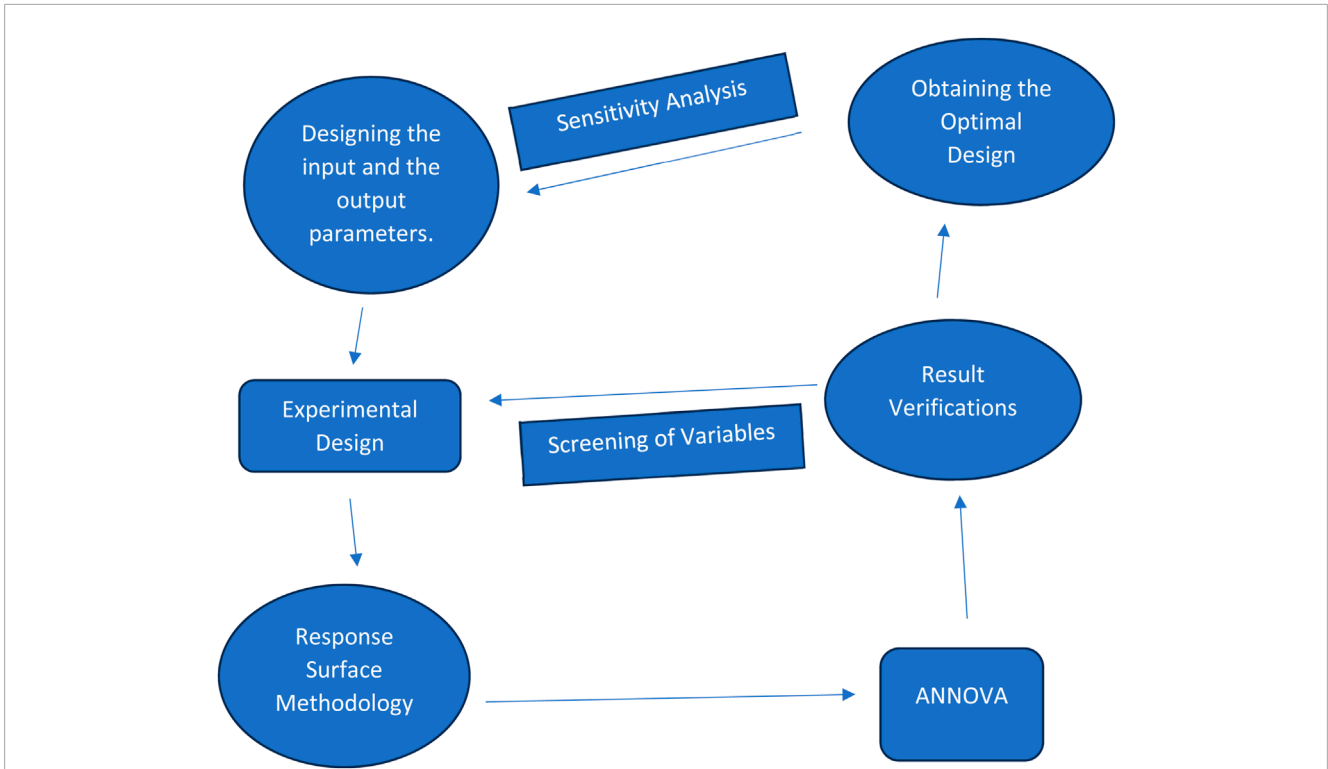


FIGURE 12 Flowchart of sensitivity analysis.

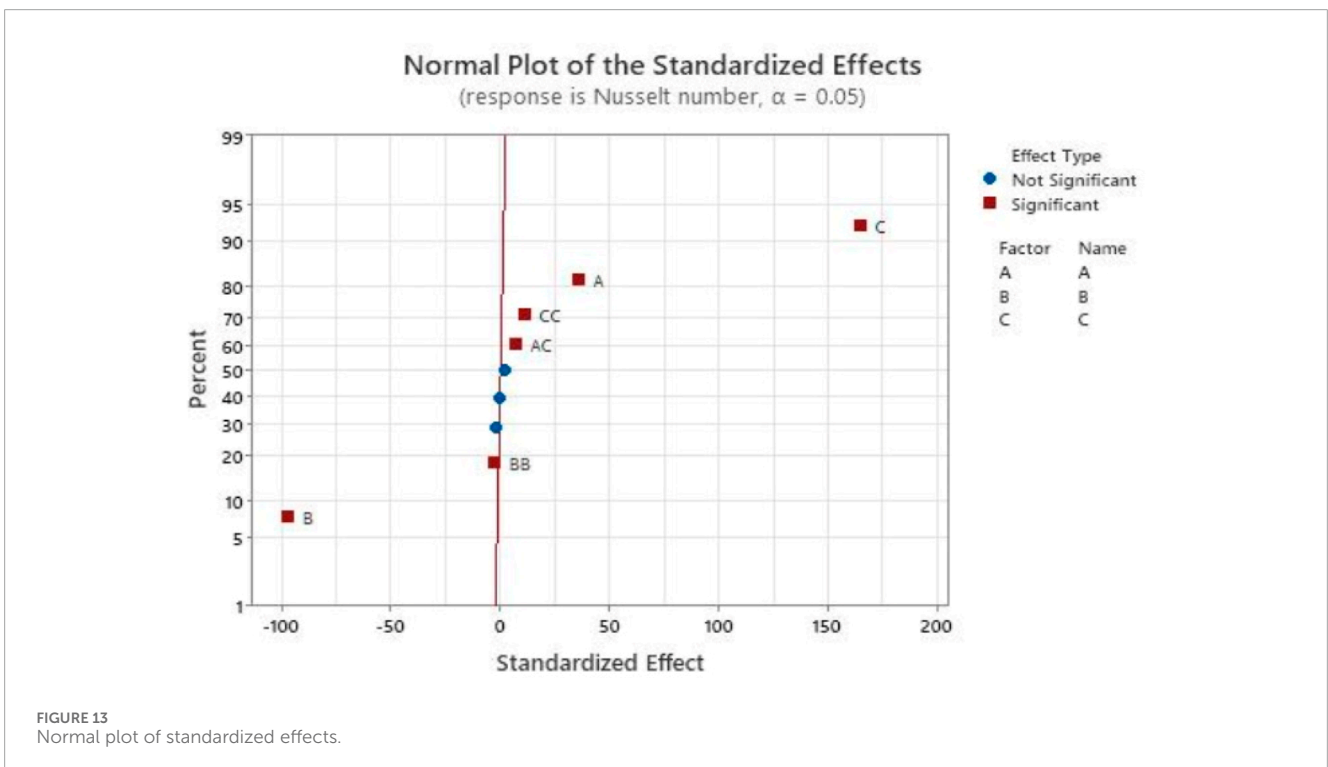
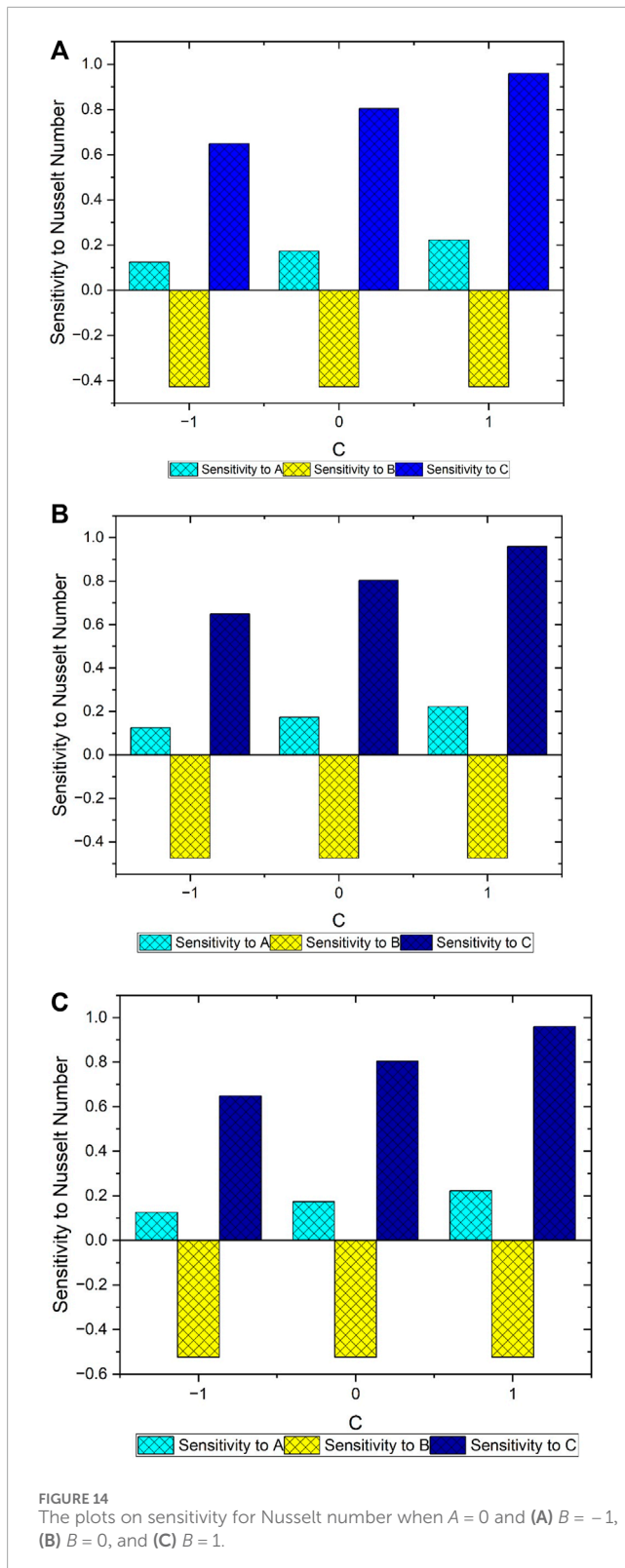


FIGURE 13 Normal plot of standardized effects.

Using Eqs (20)-(22), we evaluate the sensitivity analysis for three possible levels for each parameter and infer using the obtained results in Table 5. The sensitivity graphs shown in Figure 14 clearly portray the behavior of each of the input parameters

in influencing the Nusselt number response. In Table 8, we see that the highest sensitivity value (0.95952) occurs for $B = -1, 0, 1$ and $C = 1$ corresponding to the magnetic parameter value $A = 0$, that is, $Rd = 0.8$, while the least value (-0.52373)



occurs for $B = 1$ and $C = -1, 0, 1$ corresponding to the magnetic parameter value $A = 0$, that is, $Rd = 0.8$. So we conclude that the positive sensitivity becomes less intense with increased input parameter values. Hence, we can conclude that the sensitivity of $Re_x^{-1/2}Nu_x$ increases as we increase the values of all input parameters.

TABLE 8 Sensitivity values for $Re_x^{-1/2}Nu_x$ when $A = 0$ ($Rd = 0.8$).

B	C	$\frac{\partial(Re_x^{-1/2}C_f)}{\partial A}$	$\frac{\partial(Re_x^{-1/2}C_f)}{\partial B}$	$\frac{\partial(Re_x^{-1/2}C_f)}{\partial C}$
-1	-1	0.12493	-0.42781	0.6482
	0	0.17367	-0.42781	0.80386
	1	0.22241	-0.42781	0.95952
0	-1	0.12493	-0.47577	0.6482
	0	0.17367	-0.47577	0.80386
	1	0.22241	-0.47577	0.95952
1	-1	0.12493	-0.52373	0.6482
	0	0.17367	-0.52373	0.80386
	1	0.22241	-0.52373	0.95952

7 Conclusion

In this present study, we carried out a numerical investigation studying the effects of Rd , the heat absorption parameter, and the Falkner–Skan parameter for a 2D, hybrid nanofluid flow on a wedge geometry and conducted a sensitivity analysis using BBD. The PDEs were obtained using the Tiwari–Das model to define the problem chosen in this article. Later, they were converted to nondimensional ODEs using similarity transformations. Some of the major conclusions drawn from the results are:

- There is a decrease in the heat transfer coefficient for an increased Falkner–Skan parameter, and increasing the empirical shape factor values results in a decrease of the Nusselt number values.
- The local skin friction coefficient decreases when the concentration of nanoparticles 1 and 2 increases.
- Increasing radiation parameters result in increased Nusselt numbers.
- The high values of R^2 and $AdjR^2$ demonstrate a strong correlation between the experimental and theoretical results using regression analysis.
- The Nusselt number is most sensitive toward the Hartree pressure gradient at all levels of the other two independent factors.
- Two input parameters show a positive sensitivity toward the dependent response parameter, and one of the parameters shows a negative response, which indicates that an increase of that parameter causes the Nusselt number to decrease, which justifies the physical properties of the fluid flow.

The factors that affect the heat transfer and the skin friction coefficients for the concerning flow have been thoroughly investigated in this article, and the results are represented graphically. The motivation for this study is its contributions in the fields of magnetic drug targeting, medical sciences, and oil and petroleum industries. As a scope for future work, RSM can be paired with multiple regression analysis for three or more independent

input parameters and various other effects on a wedge model with different nanoparticle shapes and in the presence of nanoparticle aggregation. The various applications of the present study in the field of oil drilling, emulsion stabilizers, oxalic acid removal, and additives of multi-grade oils provide additional motivation for our present study. Furthermore, this problem can also be extended to apply the distinct schemes like ANN, fractional derivatives and ARA- Sumudu decomposition method etc., see [Saadeh et al. (2023a, 2023b), Chandan et al. (2024), and Qazza et al. (2023)].

Data availability statement

The raw data supporting the conclusion of this article will be made available by the authors, without undue reservation.

Author contributions

AC: conceptualization, formal analysis, methodology, software, validation, and writing—original draft. RS: formal analysis, funding acquisition, investigation, project administration, validation, and writing—review and editing. AQ: formal analysis, funding acquisition, investigation, project administration, validation, and writing—review and editing. NZ: formal analysis, funding acquisition, investigation, project administration, validation, and writing—review and editing. PJ: conceptualization, resources, supervision, writing—original draft, and writing—review and editing. UK: data curation, investigation, validation, visualization, and writing—original draft. MQ: data curation, resources, software, validation, writing—original draft, and writing—review and editing. TM: data curation, resources, software, validation, writing—original draft, and writing—review and editing.

References

- Abdelmalek, Z., Mahanthesh, B., Basir, Md F.Md, Imtiaz, M., Mackolil, J., Saeed Khan, N., et al. (2020). Mixed radiated magneto Casson fluid flow with Arrhenius activation energy and Newtonian heating effects: flow and sensitivity analysis. *Alexandria Eng. J.* 59 (5), 3991–4011. doi:10.1016/j.aej.2020.07.006
- Buongiorno, J. (2005). Convective transport in nanofluids. *J. Heat. Transf.* 128 (3), 240–250. doi:10.1115/1.2150834
- Chakraborty, A., and Janapatla, P. (2023). Scaling group analysis of a magnetohydrodynamic nanofluid flow with double dispersion and Dufour effects on a vertical wedge. *Numer. Heat. Transf. Part B Fundam.* 84 (3), 271–293. doi:10.1080/10407790.2023.2200984
- Chandan, K., Saadeh, R., Qazza, A., Karthik, K., Varun Kumar, R. S., Kumar, R. N., et al. (2024). Predicting the thermal distribution in a convective wavy fin using a novel training physics-informed neural network method. *Sci. Rep.* 14 (1), 7045.
- Cheng, P. (1979). Heat transfer in geothermal systems. *Adv. heat Transf.* 14, 1–105. doi:10.1016/S0065-2717(08)70085-6
- Choi, S., and Eastman, J. (1995). Enhancing thermal conductivity of fluids with nanoparticles. *ASME-Publications-Fed.* 231, 99–106.
- Darbari, B., Rashidi, S., and Abolfazli Esfahani, J. (2016). Sensitivity analysis of entropy generation in nanofluid flow inside a channel by response surface methodology. *Entropy* 18 (2), 52. doi:10.3390/e18020052
- Dinarvand, S., Rostami, M. N., and Pop, I. (2019). A novel hybridity model for TiO₂-CuO/water hybrid nanofluid flow over a static/moving wedge or corner. *Sci. Rep.* 9, 16290. doi:10.1038/s41598-019-52720-6
- Ghadikolaei, S. S., Yassari, M., Sadeghi, H., Hosseinzadeh, K., and Ganji, D. D. (2017). Investigation on thermophysical properties of

Funding

The author(s) declare that financial support was received for the research, authorship, and/or publication of this article. This work has been funded by the Universiti Kebangsaan Malaysia project number “DIP-2023-005.”

Acknowledgments

The authors extend their appreciation to the Deanship of Scientific Research at King Khalid University, Abha, Saudi Arabia for funding this work through General Research Project under grant number GRP/112/44.

Conflict of interest

The authors declare that the research was conducted in the absence of any commercial or financial relationships that could be construed as a potential conflict of interest.

Publisher's note

All claims expressed in this article are solely those of the authors and do not necessarily represent those of their affiliated organizations, or those of the publisher, the editors, and the reviewers. Any product that may be evaluated in this article, or claim that may be made by its manufacturer, is not guaranteed or endorsed by the publisher.

TiO₂-Cu/H₂O hybrid nanofluid transport dependent on shape factor in MHD stagnation point flow. *Powder Technol.* 322, 428–438. doi:10.1016/j.powtec.2017.09.006

Govila, R. S. R., Chamkha, A., and Rashad, A. M. (2010). “Mixed convective boundary layer flow over a vertical wedge embedded in a porous medium saturated with a nanofluid,” in 3rd International Conference on Thermal Issues in Emerging Technologies Theory and Applications (IEEE), China, 19–22 Dec. 2010 (IEEE), 445–451.

Hassan, W., Fida, M., Liu, D., Manzoor, U., and Muhammad, T. (2022). Numerical simulation of entropy generation for nanofluid with the consequences of thermal radiation and Cattaneo-Christov heat flux model. *Int. Commun. Heat Mass Transf.* 137, 106293. doi:10.1016/j.icheatmasstransfer.2022.106293

Hatami, M., and Safari, H. (2016). Effect of inside heated cylinder on the natural convection heat transfer of nanofluids in a wavy-wall enclosure. *Int. J. Heat Mass Transf.* 103, 1053–1057. doi:10.1016/j.ijheatmasstransfer.2016.08.029

Ishak, A., Roslinda, N., and Pop, I. (2007). Falkner-Skan equation for flow past a moving wedge with suction or injection. *J. Appl. Math. Comput.* 25 (1–2), 67–83. doi:10.1007/BF02832339

Kim, J., Cote, L. J., Kim, E., Yuan, W., Shull, K. R., and Hang, J. (2010). Graphene oxide sheets at interfaces. *J. Am. Chem. Soc.* 132 (23), 8180–8186. doi:10.1021/ja102777p

Kock, F., and Herwig, H. (2004). Local entropy production in turbulent shear flows: a high-Reynolds number model with wall functions. *Int. J. Heat Mass Transf.* 47 (10–11), 2205–2215. doi:10.1016/j.ijheatmasstransfer.2003.11.025

Kuilla, T., Bhadra, S., Yao, D., Kim, N. H., Bose, S., and Lee, J. H. (2010). Recent advances in graphene-based polymer composites. *Prog. Polym. Sci.* 35 (11), 1350–1375. doi:10.1016/j.progpolymsci.2010.07.005

- Kumari, M., Takhar, H. S., and Nath, G. (2001). Mixed convection flow over a vertical wedge embedded in a highly porous medium. *Heat. Mass Transf.* 37 (2-3), 139–146. doi:10.1007/s002310000154
- Lee, C., Wei, X., Kysar, J. W., and Hone, J. (2008). Measurement of the elastic properties and intrinsic strength of monolayer graphene. *Science* 321 (5887), 385–388. doi:10.1126/science.1157996
- Leong, K. Y., Razali, I. D., Ahmad, K. K., Amer, N. H., and Akmal, H. N. (2018). Thermal conductivity characteristic of titanium dioxide water based nanofluids subjected to various types of surfactants. *J. Eng. Sci. Technol.* 13 (6), 1677–1689. doi:10.1016/J.ICHEATMASSTRANSFER.2017.10.005
- Madhu, J., Saadeh, R., Karthik, K., Kumar, R. V., Kumar, R. N., Gowda, R. P., et al. (2024). Role of catalytic reactions in a flow-induced due to outer stationary and inner stretched coaxial cylinders: an application of Probabilists' Hermite collocation method. *Case Stud. Therm. Eng.* 56, 104218.
- Maïga, S. E., Nguyen, C. T., Galanis, N., and Roy, G. (2004). Micro and nano heat transfer heat transfer enhancement in forced convection laminar tube flow by using nanofluids. *Int. Symp. Adv. Comput. Heat. Transf.* 25, 24. doi:10.1615/ICHMT.2004.CHT-04.620
- Makinde, O. D., and Aziz, A. (2011). Boundary layer flow of a nanofluid past a stretching sheet with a convective boundary condition. *Int. J. Therm. Sci.* 50 (7), 1326–1332. doi:10.1016/j.ijthermalsci.2011.02.019
- Mangadlao, J. D., Cao, P., and Advincula, R. C. (2015). Smart cements and cement additives for oil and gas operations. *J. Petroleum Sci. Eng.* 129, 63–76. doi:10.1016/j.petrol.2015.02.009
- Nadeem, S., Ahmad, S., and Muhammad, N. (2018). Computational study of Falkner-Skan problem for a static and moving wedge. *Sensors Actuators B Chem.* 263, 69–76. doi:10.1016/j.snb.2018.02.039
- Natalini, G., and Sciubba, E. (1999). Minimization of the local rates of entropy production in the design of air-cooled gas turbine blades. *J. Eng. Gas Turbines Power* 121 (3), 466–475. doi:10.1115/1.2818496
- Qazza, A., Saadeh, R., Ahmed, S. A., ARA-Sumudu, (2023). Method for solving volterra partial integro-differential equations. *Appl. Math.* 17 (4), 727–734.
- Rashidi, S., Bovand, M., and Abolfazli Esfahani, J. (2015). Structural optimization of nanofluid flow around an equilateral triangular obstacle. *Energy* 88, 385–398. doi:10.1016/j.energy.2015.05.056
- Saadeh, R., Ahmed, S. A., Qazza, A., and Elzaki, T. M. (2023a). Adapting partial differential equations via the modified double ARA-Sumudu decomposition method. *Partial Differ. Equ. Appl. Math.* 8, 100539.
- Saadeh, R., Ghazal, B., and Burqan, A. (2023b). A study of double general transform for solving fractional partial differential equations. *Math. Methods Appl. Sci.* 46, 17158–17176.
- Sivakumar, N., Prasad, P. D., Raju, C. S. K., Varma, S. V. K., and Shehzad, S. A. (2017). Partial slip and dissipation on MHD radiative ferro-fluid over a non-linear permeable convectively heated stretching sheet. *Results Phys.* 7, 1940–1949. doi:10.1016/j.rinp.2017.06.016
- Sundar, L. S., Singh, M. K., Pereira, A. M., and Sousa, A. C. (2020). Augmentation of Heat Transfer of High Prandtl Number Fe 3 O 4/vacuum pump oil nanofluids flow in a tube with twisted tape inserts in laminar flow. *Heat Mass Transf.* 56, 3111–3125. doi:10.1007/s00231-020-02913-x
- Tiwari, R. K., and Das, M. K. (2007). Heat transfer augmentation in a two-sided lid-driven differentially heated square cavity utilizing nanofluids. *Int. J. Heat. Mass Transf.* 50 (9-10), 2002–2018. doi:10.1016/j.ijheatmasstransfer.2006.09.034
- Vasheghani, M., Marzbanrad, E., Zamani, C., Aminy, M., and Raissi, B. (2013). Thermal conductivity and viscosity of TiO₂- engine oil nanofluids. *Nanosci. Technol. Int. J.* 4 (2), 145–156. doi:10.1615/NanomechanicsSciTechnolIntJ.v4.i2.40
- Verma, A. K., Rajput, S., Bhattacharyya, K., Chamkha, A. J., and Yadav, D. (2022). Comparison between graphene-water and graphene oxide-water nanofluid flows over exponential shrinking sheet in porous medium: dual solutions and stability analysis. *Chem. Eng. J. Adv.* 12, 100401. doi:10.1016/j.cej.2022.100401
- White, F. M., and Majdalani, J. (2006) *Viscous fluid flow*. New York: McGraw-Hill.
- Yacob, N. A., Ishak, A., and Pop, I. (2011). Falkner-Skan problem for a static or moving wedge in nanofluids. *Int. J. Therm. Sci.* 50 (2), 133–139. doi:10.1016/j.ijthermalsci.2010.10.008
- Yih, K. A. (1998). Uniform suction/blowing effect on forced convection about a wedge: uniform heat flux. *Acta Mech.* 128, 173–181. doi:10.1007/BF01251888

Nomenclature

Quantities	Names	SI Units
C_p	Specific heat at const. pressure	$Jmol^{-1}K^{-1}$
f'	Dimensionless velocity	--
k	Thermal conductivity	$Wm^{-1}K^{-1}$
Le	Lewis number	--
m	Falkner–Skan parameter	--
Q	Heat generation parameter	--
Pr	Prandtl number	--
Re_x	Reynolds number	--
Rd	Radiation parameter	--
T	Temperature	K
T_w	Surface fluid temperature	K
T_∞	Ambient fluid temperature	K
u	x -direction velocity	ms^{-1}
U	Free stream velocity	ms^{-1}
U_∞	Constant	--
v	y -direction velocity	ms^{-1}
x, y	Coordinates	m
Greek symbols		
η	Similarity variable	--
β_1	Hartree pressure gradient	--
λ	Velocity ratio parameter	--
θ	Dimensionless temperature	--
μ	Dynamic viscosity	$kgm^{-1}s^{-1}$
ν	Kinematic viscosity	m^2s^{-1}
ρ_f	Fluid density	kgm^{-3}
ψ	Stream function	s^{-1}
Ω	Wedge angle	radians